ADVANCED FUNCTIONAL MATERIALS
www.afm-journal.de

Skin-Inspired Porous Mesh Bioelectronics with Built-In Multifunctionality for Concurrently Monitoring Heart Electrical and Mechanical Functions

*Yun Ling, Ganggang Zhao, Yajuan Su, Qian Wu, Yadong Xu, Zehua Chen, Brian Arends, Ogheneobarome Emeje, Guoliang Huang, Jingwei Xie, and Zheng Yan**

Skin exhibits nonlinear mechanics, which is initially soft and stiffens rapidly as being stretched to prevent large deformation-induced injuries. Developing skin-interfaced bioelectronics with skin-inspired nonlinear mechanical behavior, together with multiple other desired features (breathable, antibacterial, and sticky), is desirable yet challenging. Herein, this study reports the design, fabrication, and biomedical application of porous mesh bioelectronics that can simultaneously achieve these features. On the one hand, porous serpentine meshes of polyimide (PI) are designed and fabricated under the guidance of theoretical simulations to provide skin-like nonlinear mechanics and high breathability. On the other hand, ultrasoft, sticky, and antibacterial polydimethylsiloxane (PDMS) is developed through epsilon polylysine (ϵ-PL) modifications, which currently lacks in the field. Here, ϵ-PL-modified PDMS is spray-coated on PI meshes to form the core–shell structures without blocking their pores to offer ultrasoft, sticky, and antibacterial skin interfaces. And rationally designed porous hybrid meshes can not only retain skin-like nonlinear mechanical properties but also enable the integration of both soft and hard bioelectronic components for various healthcare applications. As the exemplar example, this study integrates soft silver nanowires (AgNWs) based electrophysiological sensors and rigid commercial accelerometers on multifunctional porous meshes for concurrently monitoring heart electrical and mechanical functions to provide the comprehensive information of the evolving heart status.

1. Introduction

Emerging skin-interfaced bioelectronics can reshape our future life by enabling continuous track of fitness and training, advancing fundamental understanding of dynamic human physiology and phenotypes that lead from health to diseases, and transforming healthcare from hospital-centered systems to point-of-care diagnostics.[1–6] To fully realize these potentials in the practical settings, fundamental material innovations are needed to endow skin-interfaced bioelectronics with a rich variety of desired characteristics. For example, biological tissues, such as human skin, demonstrate nonlinear mechanical behaviors, which are initially soft and stiffen rapidly as being stretched to prevent large deformation-induced injuries.[7,8] Therefore, it is desirable to develop biomimetic soft materials and/or devices with skin-inspired self-protection capabilities for various healthcare and robotic applications.[9–15] Additionally, skin-interfaced electronics should be porous and breathable to prevent sweat accumulation induced discomfort, inflammation, and biosignal loss,[4] should be antibacterial to minimize potential risks caused by foreign pathogenic bacterial contaminations,[5] and should be ultrasoft and sticky to form conformal contact with human skin for long-lasting on-skin attachment and high-fidelity biosignal recording.[6]

Recently, significant progress has been achieved in developing skin-interfaced bioelectronics with one or more of these characteristics. However, there is still a gap in the development of skin-inspired porous soft bioelectronics that can achieve all these key features. For example, nonporous materials with tissue-like nonlinear mechanics have been realized through rational designs of two-dimensional and three-dimensional skeletons and bottom-up molecular engineering, which usually demonstrate poor breathability and lack antibacterial capability.[9–15] In addition, various porous materials have been used to build breathable skin-interfaced bioelectronics, which lack rationally designed skeletons to offer skin-like nonlinear mechanics and

Y. Ling, G. Zhao, Q. Wu, B. Arends, G. Huang, Z. Yan
Department of Mechanical and Aerospace Engineering
University of Missouri
Columbia, MO 65201, USA
E-mail: yanzheng@missouri.edu
Y. Su, J. Xie
Department of Surgery-Transplant and Mary and Dick Holland Regenerative Medicine Program
University of Nebraska Medical Center
Omaha, NE 68198, USA
Y. Xu, Z. Chen, O. Emeje, Z. Yan
Department of Chemical & Biomedical Engineering
University of Missouri
Columbia, MO 65201, USA

The ORCID identification number(s) for the author(s) of this article can be found under https://doi.org/10.1002/adfm.202302681

DOI: 10.1002/adfm.202302681

self-protection capability.[16–20] Also, ultrasoft and sticky polydimethylsiloxane (PDMS) based elastomers have been developed by using various additives for skin-interfaced bioelectronic applications, which lack desired antibacterial property.[21,22] Table S1 (Supporting Information) presents a comparison of multifunctional porous materials developed in this study to other recently created functional materials for skin-interfaced applications.

To address the challenge, here, we report the design, fabrication, and biomedical application of multifunctional porous mesh bioelectronics, which are free-standing (i.e., without integration with continous elastomer substrates) and can simultaneously achieve skin-inspired nonlinar mechanics, high breathability, high stickness, and antibacterial property (Figure S1, Supporting Information). On the one hand, with the guidance of finite element analysis (FEA), we have designed and made porous PI (elastic modulus: ≈2.5GPa) meshes with skin-like nonlinear mechanics (J-shaped stress–strain curve) and high breathability. Here, rationally designed porous PI meshes can not only retain skin-like nonlinear mechanical properties but also enable the integration of both soft biosensors and hard bioelectronic components. This capability can greatly expand the applications of skin-inspired porous mesh bioelectronics in various customized healthcare. On the other hand, PDMS-based elastomers are widely used for interfacing various biological tissues because of their high biocompatibility and easy processing.[22,23] Although recent progress has been made in developing sticky PDMS, [21,22] it remains a gap to simultaneously achieve high stickiness and antibacterial properties. In this work, we have addressed this issue by simply modifying PDMS with ϵ-PL. Here, ϵ-PL is a natural broad-spectrum antimicrobial peptide and can disrupt bacterial cell membranes by electrostatic attractions.[24,25] Also, polar functional groups in ϵ-PL can inhibit the PDMS cross-linking to lower its elastic modulus to less than 40 KPa and dramatically increase its stickiness (over 25 times). Further, ϵ-PL-modified PDMS is spray-coated on PI meshes to form the core–shell structures without blocking their pores to provide ultrasoft, sticky, and antibacterial skin interfaces. As the demonstration example, a skin-interfaced bimodal cardiac monitoring system is developed by integrating soft AgNWs-based eletrophysiological sensors and commercial rigid accerometers with porous meshes. The enabled wearable system can concurrently monitor electrocardiograms (ECG) and seismocardiograms (SCG) from human chest skin and wirelessly transmit recorded signals to smartphones for graphical data display.

2. Results and Discussion

2.1. Skin-Inspired Porous Mesh Bioelectronics with Built-In Multifunctionality

Figure 1a,b presents the design concept of multifunctional porous mesh bioelectronics with skin-inspired nonlinear mechanics by using a bimodal cardiac patch as the demonstration example, which has both soft electrophysiological sensors for ECG monitoring and a hard bioelectronic component (accelerometer) for SCG recording. The fabrication process is simply illustrated in Figure S2 (Supporting Information). As demonstrated in Figure 1b, the porous PI mesh has hybrid architectures and the dominant component consists of the serpentine structures with a 175° arch angle, providing skin-like nonlinear mechanics (Figure 1c, critical strain: ≈40%), as well as working as the basis framework for spray-printing of AgNWs-based electrophysiological sensors. Besides, the central island is designed for anchoring the hard bioelectronic sensing component (i.e., accelerometer) and is not stretchable, which cannot fit human skin mechanics.[26] Therefore, we add a buffer serpentine region to relieve the island effect; the buffer region is designed with a 225° arc angle with a large critical strain (≈100%); thus, the island effect can be relieved with the buffer region[27] to fit the overall mesh mechanics. Figure 1d indicates that multifunctional porous mesh bioelectronics exhibit high breathability, whose water vapor transmission rate (≈28 mg cm^{-2} h^{-1}) is more than 40 times higher than that (≈0.7 mg cm^{-2} h^{-1}) of the PI film with the same thickness (25 μm thick) and is comparable to that of an open bottle (≈40 mg cm^{-2} h^{-1}). In addition, ϵ-PL modified PDMS demonstrates high on-skin adhesion force (≈80 Nm^{-1}), can hold a 20-gram weight (Figure 1e), and exhibits about 90% bactericidal efficacies against both *Pseudomonas aeruginosa* (PA) and Gram-positive Methicillin-resistant *Staphylococcus aureus* (MRSA) (Figure 1f). Multifunctional porous mesh bioelectronics coated with ϵ-PL modified PDMS can stay on human skin for 3 days without delamination (Figure S3, Supporting Information). More details regarding the design and testing of the porous PI mesh skeletons, the synthesis and characterization of ϵ-PL-modified PDMS, and the assembly and evaluation of biomodal skin-interfaced cardiac monitoring systems are provided in the following sections.

2.2. FEA-Guided Design of Porous PI Meshes with Skin-Inspired Nonlinear Mechanics

As illustrated in Figure S4 (Supporting Information), biological tissues (e.g., human skin) usually demonstrate three-stage, J-shaped, nonlinear mechanical responses,[7,8] which are rooted from their undulated fibrous structures. Breifly stated, the folded fibrous structures gradually expands in the early stage of stretching. When a specific strain is reached, fibrous structures are straightened and biological tissues rapidly stiffen. In this work, we use the FEA-guided, rationally designed porous mesh of ultrathin PI (25 μm thick; elastic modulus: 2.5 GPa) to mimic the skin nonlinear mechanics. **Figure 2**a shows the geometric parameters associated with the porous mesh unit cell, including the arc angle (θ), width (W), and radius (R). The mechanics of porous PI meshes is determined by the arc angle and normalized width ($W^* = W/R$) at a fixed thickness. Based on our experimental and simulation results, the porous PI mesh with the arc angle of 175° and the normalized width of 0.15 can fit the nonlinear mechanics of human chest skin (Figure 2b). As demonstrated in Figure 2c, FEA simulations can quantitively capture the porous mesh deformations under stretching. Analogous to undulated fibrous tissues, porous PI meshes first undergo unfolding upon stretching and then experience a transition into the stretching-dominated deformation when meshes along the loading direction are straightened. The transition point is defined as the critical strain (≈40% for the design in Figure 1b). Besides, the spray-coating of both ϵ-PL-modified PDMS and AgNWs has negligible effects on the nonlinear mechanical properties of porous PI mesh skeletons (Figure S5, Supporting Information), mainly due

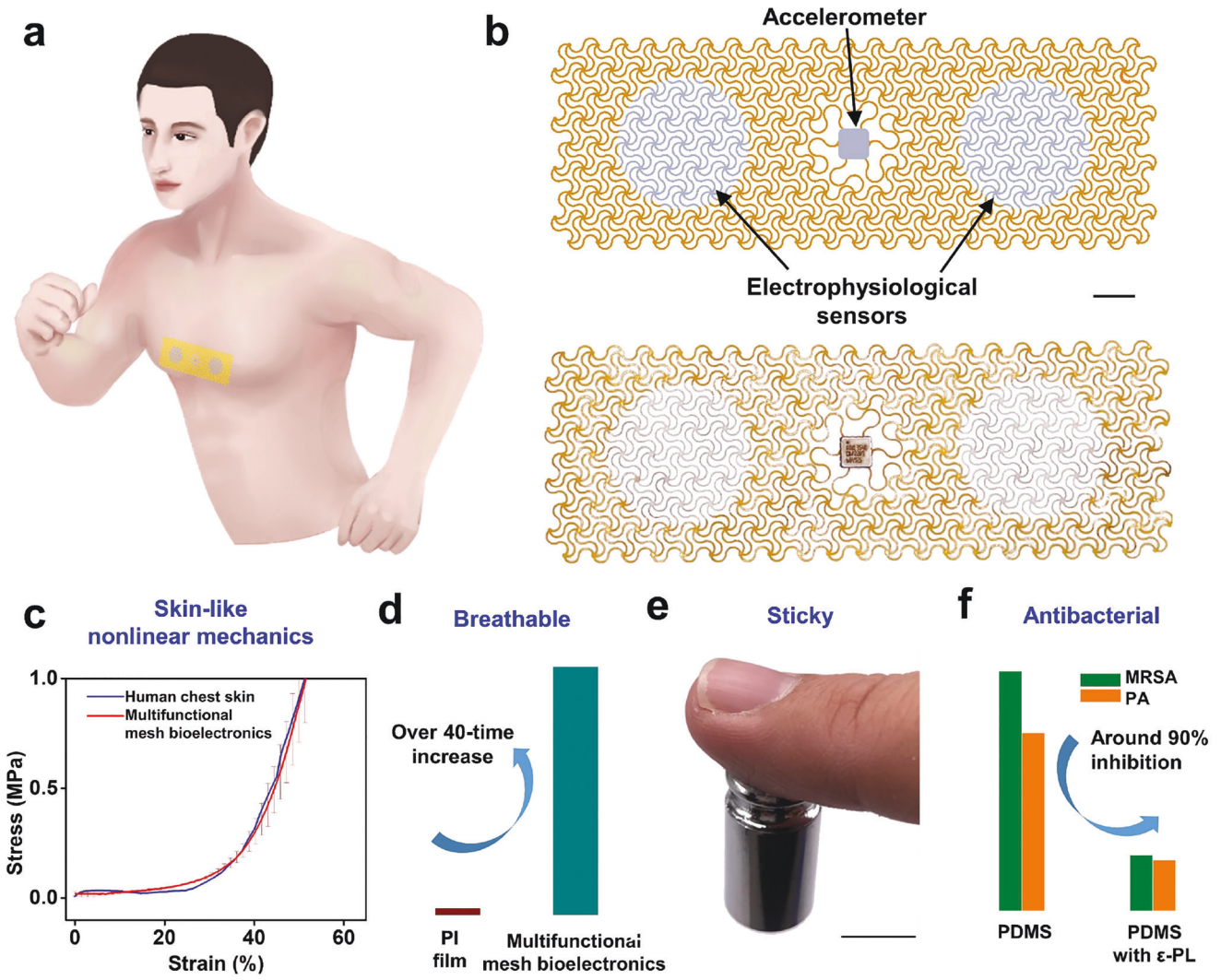

Figure 1. Skin-inspired porous mesh bioelectronics with built-in multifunctionality. a) Illustration of the bimodal cardiac patch based on skin-inspired porous meshes, which can be attached on chest skin for concurrent monitoring of heart electrical (i.e., electrocardiograms (ECG)) and mechanical (i.e., seismocardiograms (SCG)) biosignals. b) Scheme (top) and optical image (bottom) of the bimodal cardiac patch, consisting of rationally designed, hybrid porous polyimide (PI) meshes, whose surface is coated with ultrasoft, sticky, and antibacterial polydimethylsiloxane (PDMS) modified with epsilon polylysine (ϵ-PL) for skin interfacing. Here, silver nanowires (AgNWs) based electrophysiological sensing electrodes are spray-printed onto the desired locations of porous meshes and a 3-axis accelerometer (ADXL 354) is bonded on the center island. The porous mesh is designed with a 175° arc angle to offer skin-inspired nonlinear mechanical property. And the island is used to host hard SCG sensing component (i.e., accelerometer), which is not stretchable. Thus, a buffer serpentine region with a 225° arc angle is incorporated to relieve the island effect and to fit the overall mesh mechanics. c) Stress–strain curves of human chest skin and multifunctional porous mesh bioelectronics, which agree well with each other. The breathability (i.e., water vapor transmission rate) of porous mesh bioelectronics is over 40 times higher than that of the polyimide (PI) film with the same thickness (d). PDMS modified with ϵ-PL (5% by weight) demonstrates high stickiness and outstanding antibacterial performance, which can hold a 20-gram weight (e) and exhibits ≈90% bactericidal efficacy against both gram-negative PA and gram-positive MRSA (f). Error bars in (c) are determined from three samples. Scale bars in (b) and (e) are 5 mm and 1 cm, respectively.

to their trace coating amaounts and low modulus as compared to PI. For the practical biomedical applications, both soft bioelectronic sensors (e.g., AgNWs-based electrophysiological sensing electrodes) and hard bioelectronic components (e.g., accelerometer) are needed to collect comprehensive information of the body status. To satisfy this requirement, we have further developed the hybrid porous mesh with a central island, which can be adopted to host hard bioelectronic components (Figure 2d,e and Figure S6, Supporting Information). The central island is not stretchable. Therefore, we add a buffer region to relieve the island effect; the buffer region is designed with the 225° arc angle and 0.15 normalized width with a large critical strain (≈100%); thus, the island effect is relieved with the buffer region to fit the overall porous mesh mechanics. Also, FEA simulations agree well with experimental results and can quantitively capture the deformation of the hybrid porous mesh under stretching (Figure 2e). Thanks to the porous design, the PI mesh is highly breathable (Figure 2f) and transparent (Figure 2g). For instance, its water

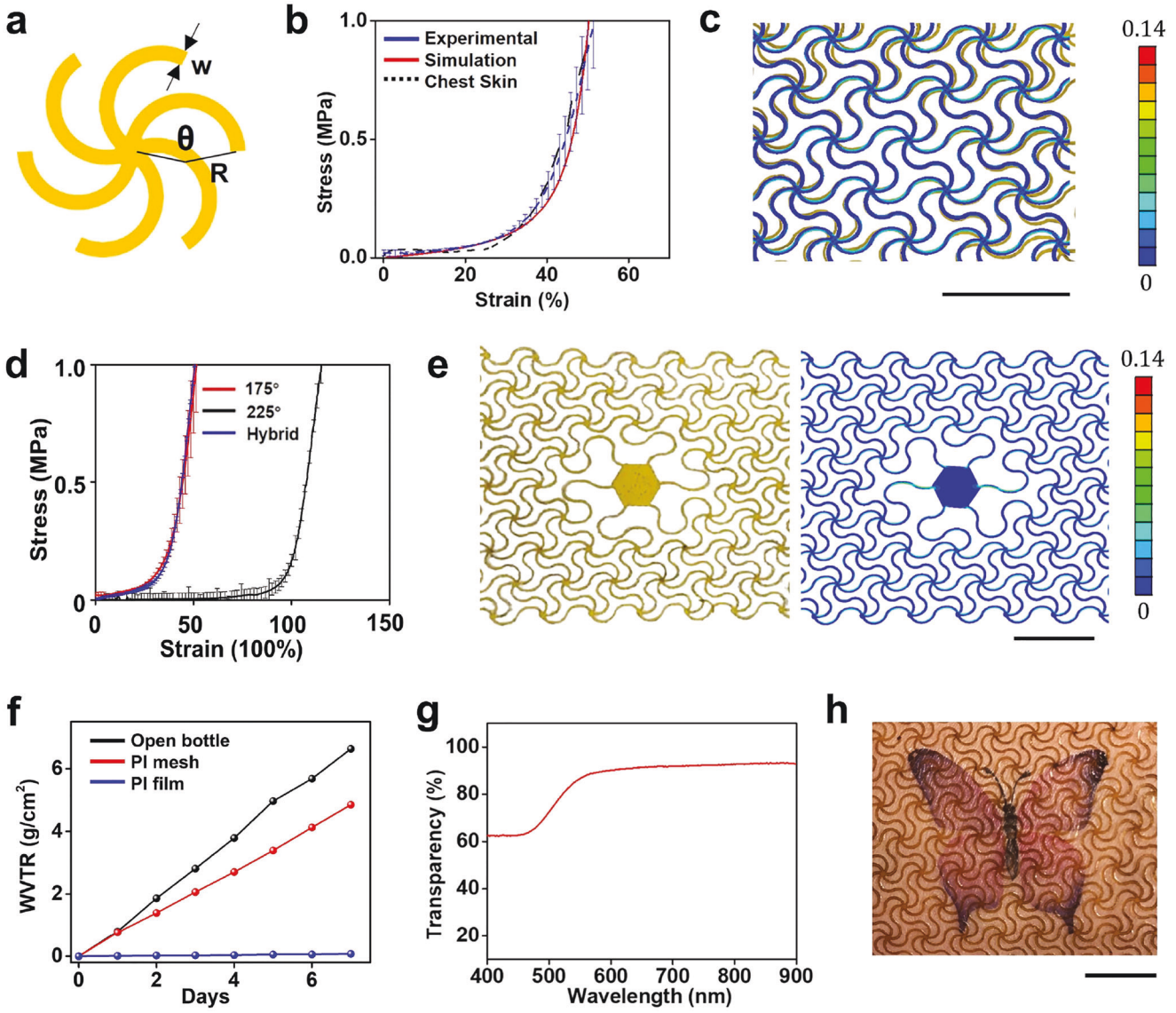

Figure 2. Breathable porous PI meshes with programmed skin-inspired nonlinear mechanics. a) Schematic illustration of geometric parameters associated with the mesh unit cell, including the arc angle (θ), width (W), and radius (R). The mechanics of porous meshes are determined by the arc angle and the normalized width ($W^* = W/R$) at a fixed thickness (25 µm for this study). b) Experimentally measured and FEA stimulated stress–strain curves of porous meshes (arc angle: 175°, normalized width: 0.15) that can fit the nonlinear mechanics of human chest skin. c) Optical image of the 20% stretched porous mesh overlapped with the corresponding simulation, indicating quantitive agreement. d) Stress–strain curves of the porous mesh with an arc angle of 175° and normalized width of 0.15, the porous mesh with an arc angle of 225° and normalized width of 0.15, and the hybrid structure as schematically illustrated in Figure S6 (Supporting Information). In the hybrid structure, a buffer serpentine region with a 225° arc angle is used to connect the serpentine region with a 175° arc angle and the center island to relieve the island effect. e) Optical image (left) and corresponding FEA simulation (right) of the 20% stretched hybrid porous mesh, indicating quantitive agreement. f) Water vapor transmission rates (WVTR) of the PI film, the porous PI mesh, and an open bottle. g) Optical transparency of the porous PI mesh with skin-like mechanics. h) Optical image of the porous mesh attached on human skin, clearly showing the butterfly sticker underneath the mesh. Error bars in (b) and (d) are determined from three samples. Color bars in (c) and (e) indicate strain distributions in FEA simulated results. Scale bars: 1 cm.

vapor transmission rate (≈28 mg cm^{-2} h^{-1}) is over 40 times higher than that (≈0.7 mg cm^{-2} h^{-1}) of the PI with the same thickness and is comparable to that of an open bottle (≈40 mg cm^{-2} h^{-1}). Figure 2h indicates that the butterfly tattoo sticker, on the skin, is clearly visible through the PI mesh. Here, high optical transparency will allow users to monitor skin conditions (e.g., rashes) underneath skin-interfaced bioelectronic patches. Notably, the spray-coating of ϵ-PL-modified PDMS has negligible effects on the breathability and transparency of the PI mesh (Figure S7, Supporting Information). Figure S8 (Supporting Information) shows porous PI meshes coated with ϵ-PL-modified PDMS can form conformal contact with underneath human skin and naturally follow the skin deformations under compression and stretching without delamination.

2.3. Synthesis and Characterization of ϵ-PL-Modified PDMS

Sticky PDMS can be made using various methods.[21,22] However, sticky PDMS with outstanding antibacterial property is still lacking, which can minimize risks of pathogenic bacterial infections during home-based long-term applications of soft bioelectronics.[5] Here, we prepare sticky and antibacterial PDMS by simply adding a small fraction of commercially available ϵ-PL. More details are provided in the Experimental Section. As illustrated in **Figure 3**a and Figure S9 (Supporting Information), polar functional groups in ϵ-PL can interact with the Pt catalyst in the PDMS curing agent, thus hindering the cross-linking reaction of PDMS and resulting in heterogeneously cross-linked networks (i.e., composing of both high cross-linked and low cross-linked PDMS).[21,22] The obtained PDMS can stick to human skin (Figure 3b) and is highly stretchable (Figure 3c), which are the key form factors for skin-interfaced applications. Here, we compare the pure PDMS (base-to-crosslinker ratio: 10:1) and PDMS (base-to-crosslinker ratio:10:1) loaded with various amounts of ϵ-PL (1%, 2.5% and 5% by weight). As shown in Figure 3d, as compared to pure PDMS, ϵ-PL-modified PDMS exhibits higher stretchability and lower elastic modulus, which are more suitable for skin-interfaced applications. For example, the pure PDMS's elastic modulus is ≈1 MPa and its failure strain is ≈200%. By contrast, the elastic modulus of ϵ-PL-modified PDMS (5%) is ≈40 KPa and it can be stretched to over 500% without breaking (Figure 3c). Furthermore, ϵ-PL-modified PDMS demonstrates high on-skin adhesion forces. For instance, the on-skin adhesion force of ϵ-PL-modified PDMS (5%) is ≈80 N m^{-2}, over 25 times higher than that of pure PDMS (≈3 N m^{-2}). Notably, sticky PDMS can also be enabled by reducing cross-linker amounts, which demonstrates poor mechanical property as compared with that of ϵ-PL-modified PDMS (Figure S10, Supporting Information).[22] The high on-skin adhesion force of ϵ-PL-modified PDMS arises from its enahced visoelasticty (Figure S11, Supporting Information). In brief, ϵ-PL-modified PDMS demonstrates flowability and can form conformal contact with human skin rich with microstructures, which can increase the contact area and thereby maximizes van der Waals forces (Figure S12, Supporting Information). And ϵ-PL-modified PDMS also exhibits good transparency (Figure S13, Supporting Information) and long-term stability of on-skin attachment (Figure S14, Supporting Information).

In this study, Gram-negative PA and Gram-positive MRSA were used for antibacterial tests and the bactericidal efficacy was determined by the colony count method.[28] As illustrated in Figure 3f, pure PDMS shows negligible antibacterial capability, and increasing ϵ-PL contents can enhance the bactericidal efficacy. Here, PDMS with 5% ϵ-PL exhibits around 90% bactericidal efficacies against PA and MRSA because ϵ-PL can disrupt bacterial membrane structures.[24,25] To examine the biocompatibility of ϵ-PL-modified PDMS, we further performed cytotoxicity tests with the human dermal fibroblast (HDF) cell line. Figure 3g indicates that there are no significant differences ($p > 0.05$) in cell viability among the cells cultured with ϵ-PL-modified PDMS and on tissue culture polystyrene (control) after 1-day, 3-day, and 5-day cell culturing. And the fluorescence micrographs (Figure 3f) show regular live cell (green) morphologies and rare dead cells (red) after 5-day culturing with ϵ-PL-modified PDMS and on the control sample. These results demonstrate that ϵ-PL-modified PDMS has negligible cytotoxicity and outstanding biocompatibility. Notably, with high ϵ-PL contents, the needed PDMS curing time is prolonged. To balance the curing time and performance, in this study, PDMS with 5% ϵ-PL is spray-coated on porous PI meshes for the preparation of skin-inspired multifunctional porous mesh bioelectronics.

2.4. Concurrent Monitoring of Heart Electrical and Mechanical Functions

Heart diseases are the leading cause of death in the world and more than 90% of heart diseases are treatable through early detections and timely interventions.[29,30] Continuous monitoring of cardiac electrical activities via ECG outside clinical settings plays an indispensable role in early diagnosis of various heart diseases.[31–33] Concurrent measurement of SCG (**Figure 4**a) can reveal essential information of heart mechanics absent from ECG (e.g., myocardial activity and valve motions) to benefit early detections of various cardiac complications.[34–36] Here, we have further developed a skin-interfaced bimodal cardiac monitoring system by taking advantage of the rationally designed multifunctional porous PI meshes, which can simultaneously record ECG and SCG signals (Figure 1b). In addition, the bimodal cardiac patch can be connected to the mobile data acquisition circuit clipped on clothes (Figure S15, Supporting Information) for in situ data processing and wireless data transmission. The block diagram of the mobile data acquisition module is shown in Figure 4b, and the detailed design and off-the-shelf electronic components are provided in Figure S16 and Table S2 (Supporting Information). AgNWs are spray-printed onto porous meshes as the sensing electrodes for ECG recording. The scanning electron microscopy (SEM) image in Figure 4c shows that AgNWs are effectively embedded in the polymer matrix of ϵ-PL-modified PDMS to introduce conducting properties. Figure 4d demonstrates that spray-printed AgNWs exhibit high stability and small resistance changes (<10%) under cyclic stretching tests. Also, Figure S17 (Supporting Information) shows that after 100-time peeling-off tests using Scotch tape, there are no significant changes in the morphology and electrical conductivity of spray-printed AgNWs, and no AgNWs are observed on the Scotch tape, indicating the robust integration of AgNWs with serpentine PI meshes coated with ϵ-PL-modified PDMS. And a commercially available three-axis accelerometer (ADXL 354), bonded on the central island of the porous PI mesh, for SCG (*Z*-axis signals) recording. Figure 4e provides ECG and SCG signals concurrently measured from a human subject using the skin-interfaced biomodal cardiac monitoring system. And the qualities of recorded biosignals are comparable to those measured using commercial devices (Figure S18, Supporting Information). Some key features are highlighted in the magnified views of the recorded ECG and SCG signals (Figure 4f), which can reveal meaningful information for the assessment of cardiac functions. For example, the time interval from the onset of the QRS to the point of the peak intensity of S1 corresponds to the time required for the left ventricle to achieve sufficient pressure to force the mitral valve to close, and its prolongation indicates the potential systolic heart failure.[35] Besides, 24-h continuous monitoring of

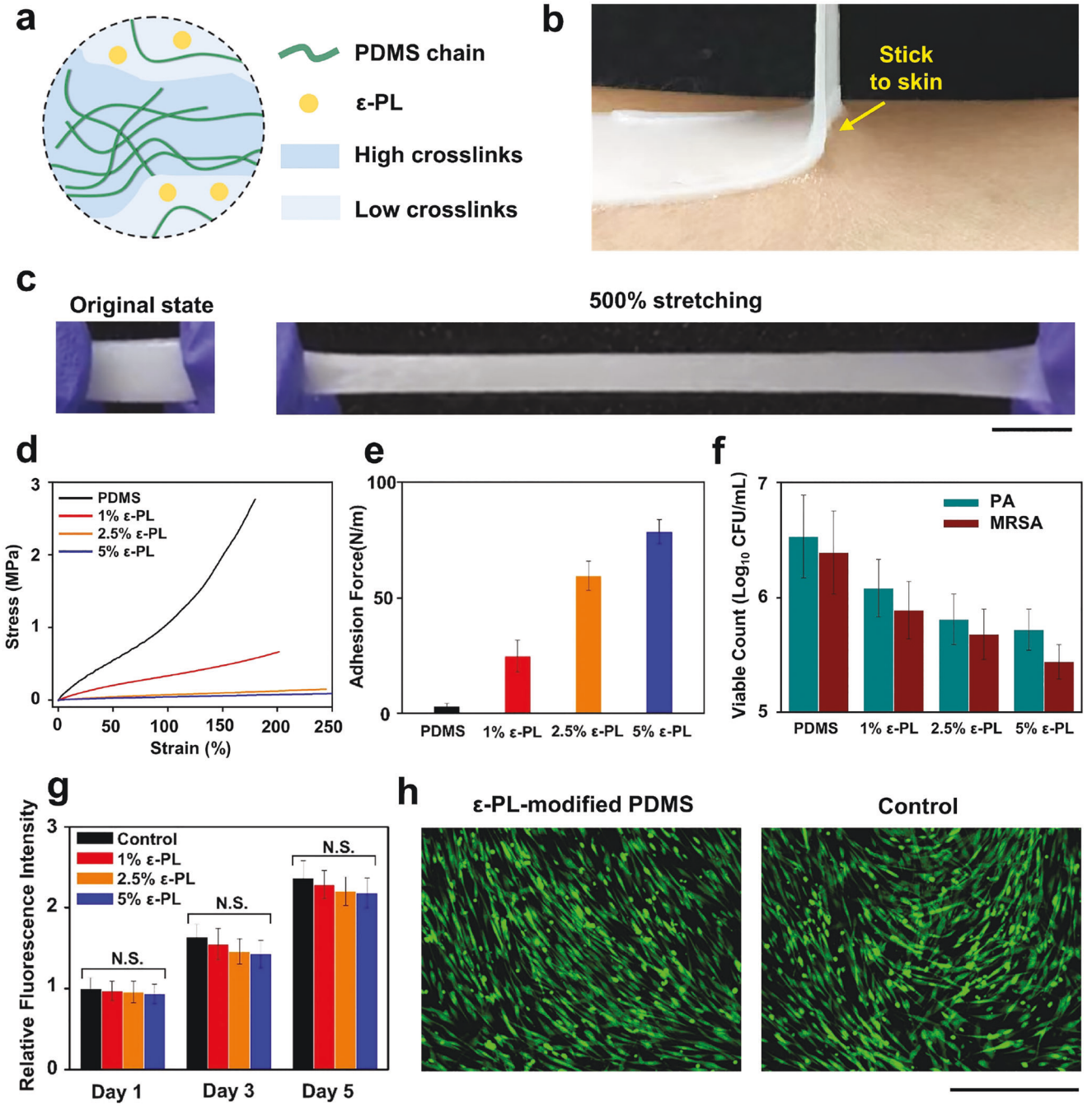

Figure 3. Sticky and antibacterial polydimethylsiloxane (PDMS) modified with epsilon polylysine (ε-PL). a) Conceptual illustration of ε-PL-modified PDMS with heterogeneous crosslinking networks. (b) Photograph indicating the strong adhesion between ε-PL-modified PDMS and skin. c) Photographs of ε-PL-modified PDMS under the original state and 500% stretching. d) Stress–strain curves of the pure PDMS and PDMS with 1%, 2.5%, and 5% ε-PL. e) Adhesion forces measured between the skin and the pure PDMS and PDMS with different ε-PL fractions. f) Antibacterial performances of the pure PDMS and PDMS with different ε-PL fractions. g) Relative fluorescence intensities of the control sample and PDMS with different ε-PL fractions after 1-day, 3-day, and 5-day incubations of human dermal fibroblast (HDF) cells. h) Fluorescent images of HDF cells cultured with the ε-PL-modified PDMS (left) and the control sample (right) for 5 days. Error bars in (e), (f), and (g) are determined from three samples. Scale bars in (c) and (h) are 5 mm and 500 μm, respectively.

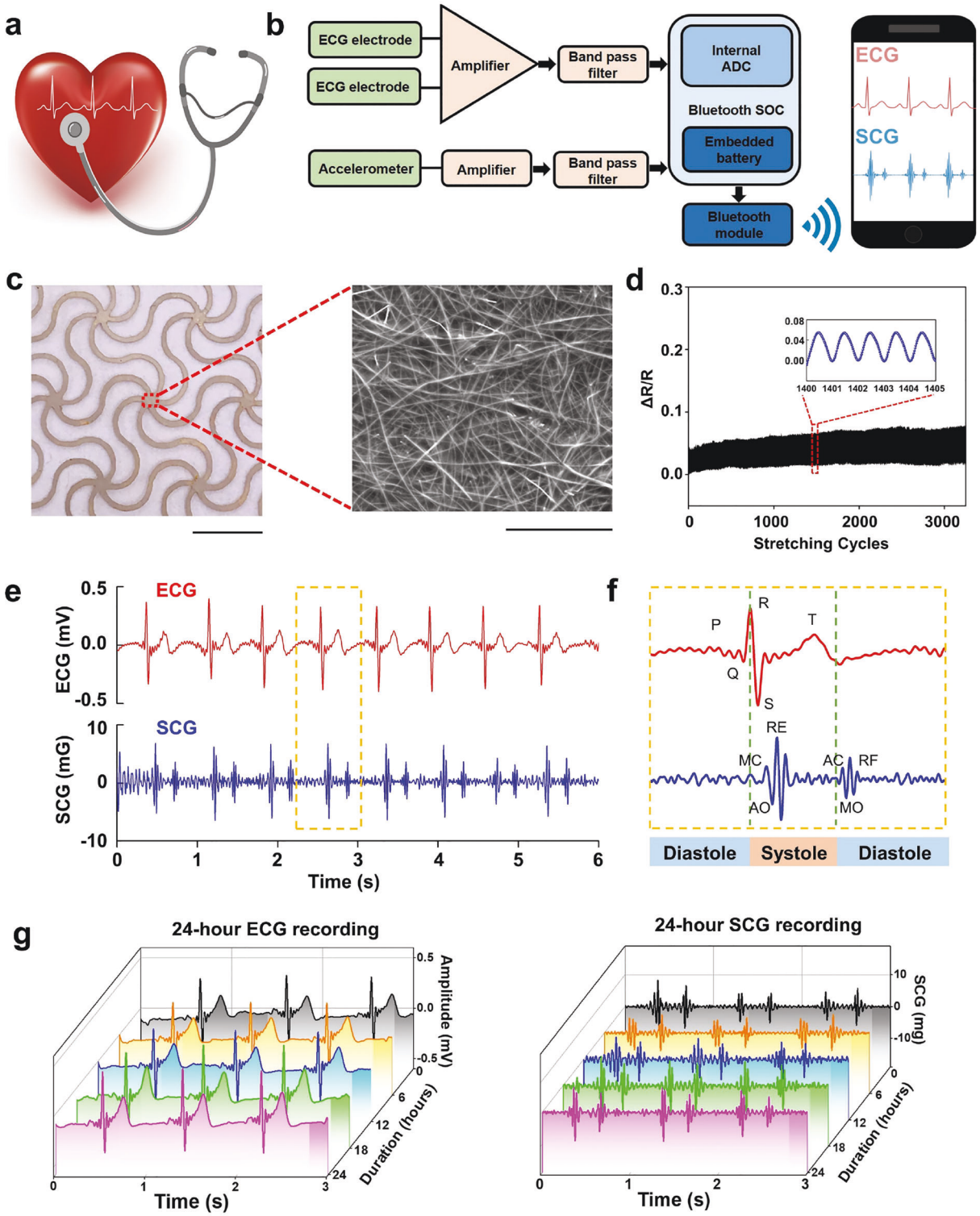

Figure 4. Concurrent monitoring of heart electrical and mechanical functions. a) Conceptual illustration of simultaneously recording cardiac electrical (ECG) and mechanic (SCG) biosignals. b) The system-level block diagram of the mobile data acquisition circuit, and illustration of graphic data display of ECG and SCG on the smartphone. c) Optical (left, scale bar: 5 mm) and scanning electron microscopy (SEM; right, scale bar: 5 μm) images of ECG sensing electrodes, fabricated by spray-printing of silver nanowires (AgNWs) on the selected locations of porous polyimide (PI) meshes coated with epsilon polylysine (ε-PL) modified polydimethylsiloxane (PDMS). d) Relative resistance changes of AgNWs on PI meshes subjected to cyclic stretching (up to 40%), showing high stablity and small electrical resistance changes. e) ECG (top) and SCG (bottom), measured simultaneously using porous mesh bioelectronics illustrated in Figure 1b and Figure S15 (Supporting Information). f) Magnified views of ECG and SCG signals. MC, mitral valve closure; AO, aortic valve opening; RE, rapid ventricular ejection; AC, aortic valve closure; MO, mitral valve opening; RF, rapid ventricular filling. g) 24-h continous monitoring of ECG (top) and SCG (bottom) signals from a healthy human subject.

ECG and SCG (Figure 4g) indicates the long-term stability and fidelity of the skin-interfaced biomodal cardiac monitoring system. Also, Figure S19 (Supporting Information) shows that the device can still record high-fidelity biosignals during human motions.

3. Conclusion

In summary, we have developed skin-inspired porous mesh bioelectronics with unprecedented built-in multifunctionality. And, FEA simulations can be used to guide the design and fabrication of porous PI mesh skeletons to provide skin-inspired nonlinear mechanics, high breathability, and anchoring sites of both soft and hard bioelectronic components. In addition, ϵ-PL-modified PDMS is developed and spray-coated on porous PI meshes to form core–shell structures without blocking their pores to offer ultrasoft, sticky, and antibacterial skin interfaces. The obtained skin-interfaed biomodal heart monitoring system can concurrently monitor ECG and SCG signals in a long-term manner to provide meaningful information for the evolving heart status. The design principles and fabrication methods, reported in this paper, can be further adopted for the development of other types of skin-interfaced and implanted bioelectronics, which can nonlinearly mechanically match targeted biological tissues, form ultrasoft, sticky, and antibacterial biotic–abiotic interfaces, and offer customized functions for various diseased conditions.

4. Experimental Section

Materials and Fabrications: PDMS (Sylgard 184, Dow), silver paint, tetrahydrofuran (THF), and isopropanol (IPA) were purchased from MilliporeSigma. ϵ-PL (25 w/v% aqueous solution, 25–35 mer, molecular weight: 3222-4503 Da) was provided by JNC Corp (Tokyo, Japan). And PI films (Kapton HN-100, 25 µm thick) were provided by Dupont. AgNWs (Agnw-40, IPA carrier) were purchased from ACS Material. All these materials were used as received.

Serpentine meshes of PI were made by CO_2 laser cutting (VLS2.30 universal laser system) on the commercial PI film (25 µm thick). ϵ-PL-modified PDMS was prepared by mixing the ϵ-PL aqueous solution and PDMS (base-to-crosslinker ratio: 10:1) and curing the precursors at 80 °C for 1–2 h. The fraction of ϵ-PL in the PDMS composite can be adjusted by changing the amount of the ϵ-PL aqueous solution. And the air-spraying ink of ϵ-PL-modified PDMS was prepared by mixing its precurosor with THF (content: 30% by weight) and spray-printed onto PI serpentine meshes using a commercial airbrush (G222; Master Airbrush). AgNWs were diluted by IPA with a weight ratio of 1:10 and spray-printed on porous PI meshes, which were precoated with partially cured ϵ-PL-modified PDMS, through shadow masks using the commercial airbrush. The coating amounts of ϵ-PL-modified PDMS and AgNWs were 0.06 and 0.8 mg cm^{-2}, respectively. Accelerometers were bonded onto central PI islands using ϵ-PL-modified PDMS. Silver paints were used to connect the bisensors with liquid metal-based conductive wires,[37] as well as to connect conductive wires with data acquisition modules.

Characterizations, Measurements, and Numerical Simulations: SEM images were taken with an FEI Quanta 600 FEG Environmental SEM. And on-skin adhesion forces were determined via peeling tests following ASTM D3330 standards. Strain–stress curves were acquired using a Mark-10 ESM303 tensile tester. Optical transparency was tested by a UV–VIS spectrometer (Lambda 35, PerkinElmer). Water-vapor transmission rates were estimated by measuring the weight loss of water by attaching the sample to the opening of a bottle with pure water. The testing procedure was based on ASTM E96. And FEA simulations were conducted by commercial software ABAQUS (SIMULIA, Providence RI) to analyze deformations and stress–strain responses of mesh bioelectronics.

Cytotoxic Tests: The cytotoxicity was studied following a contact mode protocol with HDF.[38] The elastomer samples were cut into 1 cm diameter disks and sterilized with 70% ethanol, followed by rinsing with sterilized PBS. Cells (5×10^4 cells cm^{-2}) were cultured in a 24-well culture plate using fibroblast growth kit-low serum (ATCC, USA). After 6 h for cell attachment on the culturing plate, the pre-sterilized samples were carefully transferred to the wells containing cells, ensuring they were faced to the cells. The plates containing cells and samples were cultured for 5 days, and the culture medium was changed every 2 day. On the first, third, and fifth day, the viability of the HDF cells contacting with samples was determined with Alamar blue assay and LIVE/DEAD assay. Alamar blue assay (Thermo Fisher, USA) was implemented following the protocol provided by the manufacturer. HDF cells were also stained using LIVE/DEAD cell viability kit (Thermo Fisher) and then examined with an inverted fluorescence microscope (Leica, Germany).

Antimicrobial Evaluations: The antimicrobial performances of the elastomer samples were determined using a reported protocol.[28] Gram-positive Methicillin-resistant *Staphylococcus aureus* USA300 (MRSA) and Gram-negative *Pseudomonas aeruginosa* E411-17 (PA) were inoculated in LB medium overnight at 37 °C, then recultured in fresh medium and grown to OD600 = 0.5. The two test inoculums were diluted to a final concentration of 1×10^8 CFU mL^{-1}, and 10 µL of the bacteria suspension was spread over samples, which were then covered with other samples and gently pressed to spread the inoculums over the entire surface of the samples. The inoculated samples were incubated at 37 °C for 2 h. Then 1 mL PBS was added into the 35 mm Petri dishes, which contain the testing samples, to wash out the survived microbe. And the bacteria suspensions were plated for colony forming unit (CFU) counts. This test was repeated with at least triplicate samples. The Kill% ratio was calculated by the CFU (treated)/CFU (control).

Experiments on Human Subjects: The on-body evaluations of skin-interfaced devices on human subjects were conducted under the approval from Institutional Review Board at the University of Missouri-Columbia (number:2010272). All human subjects gave written and informed consent before participation in the studies.

Statistical Analysis: The statistical analysis was performed using GraphPad Prism 8.0 software. Differences among groups were evaluated using one-way ANOVA followed by Tukey's multiple comparisons test. The values of $p < 0.05$ were considered statistically significant.

Supporting Information

Supporting Information is available from the Wiley Online Library or from the author.

Acknowledgements

Y.L. and G.Z. contributed equally to this work. Z.Y. acknowledges the financial support from the startup fund of the University of Missouri-Columbia and National Science Foundation (award number: 2045101). J.X. acknowledges the financial support from the startup fund of the University of Nebraska Medical Center. G.H. acknowledges the Air Force Office of Scientific Research, USA under Grant No. AF 9550-20-1-0279 with Program Manager Dr. ByungLip (Les) Lee and the Office of Naval Research, USA under Grant No. FA9550- 563 21-1-0226 with Program Manager Dr. Anisur Rahman.

Conflict of Interest

The authors declare no conflict of interest.

Data Availability Statement

The data that support the findings of this study are available from the corresponding author upon reasonable request.

Keywords

adhesives, antibacterial, breathable, heart monitoring, skin-like nonlinear mechanics

Received: March 8, 2023
Revised: April 26, 2023
Published online: June 9, 2023

[1] D. H. Kim, N. Lu, R. Ma, Y. S. Kim, R. H. Kim, S. Wang, J. Wu, S. M. Won, H. Tao, A. Islam, K. J. Yu, T. i. Kim, R. Chowdhury, M. Ying, L. Xu, M. Li, H. J. Chung, H. Keum, M. Martin, P. Liu, Y. W. Zhang, F. G. Omenetto, Y. Huang, T. Coleman, J. A. Rogers, *Science* **2011**, *333*, 838.
[2] T. Ray, J. Choi, A. J. Bandodkar, S. Krishnan, P. Gutruf, L. Tian, R. Ghaffari, J. A. Rogers, *Chem. Rev.* **2019**, *119*, 5461.
[3] K. Sim, Z. Rao, F. Ershad, C. Yu, *Adv. Mater.* **2020**, *32*, 1902417.
[4] T. Someya, M. Amagai, *Nat. Biotechnol.* **2019**, *37*, 382.
[5] S. Xu, A. Jayaraman, J. A. Rogers, *Nature* **2019**, *571*, 319.
[6] S. Liu, Y. Rao, H. Jang, P. Tan, N. Lu, *Matter* **2022**, *5*, 1104.
[7] C. Storm, J. J. Pastore, F. C. MacKintosh, T. C. Lubensky, P. A. Janmey, *Nature* **2005**, *435*, 191.
[8] G. C. Engelmayr, M. Cheng, C. J. Bettinger, J. T. Borenstein, R. Langer, L. E. Freed, *Nat. Mater.* **2008**, *7*, 1003.
[9] H. Zhang, X. Guo, J. Wu, D. Fang, Y. Zhang, *Sci. Adv.* **2018**, *4*, eaar8535.
[10] D. Yan, J. Chang, H. Zhang, J. Liu, H. Song, Z. Xue, F. Zhang, Y. Zhang, *Nat. Commun.* **2020**, *11*, 1180.
[11] J. Liu, D. Yan, W. Pang, Y. Zhang, *Mater. Today* **2021**, *49*, 324.
[12] K. Jang, H. U. Chung, S. Xu, C. H. Lee, H. Luan, J. Jeong, H. Cheng, G. Kim, S. Y. Han, J. W. Lee, J. Kim, M. Cho, F. Miao, Y. Yang, H. N. Jung, M. Flavin, H. Liu, G. W. Kong, K. J. Yu, S. Rhee, J. Chung, B. Kim, J. W. Kwak, M. H. Yun, J. Y. Kim, Y. M. Somng, U. Paik, Y. Zhang, Y. Huang, J. A. Rogers, et al., *Nat. Commun.* **2014**, *6*, 6566.
[13] Y. Ling, W. Pang, J. Liu, M. Page, Y. Xu, G. Zhao, D. Stalla, J. Xie, Y. Zhang, Z. Yan, *Nat. Commun.* **2022**, *13*, 524.
[14] M. Vantankhah-Varbosfaderani, W. F. M. Daniel, M. H. Everhart, A. A. Pandya, H. Liang, K. Matyjaszewski, A. V. Dobrynin, S. S. Sheiko, *Nature* **2017**, *549*, 497.
[15] M. Vantankhah-Varbosfaderani, A. N. Keith, Y. Cong, H. Liang, M. Rosenthal, M. Sztucki, C. Clair, S. Magonov, D. A. Ivanov, A. V. Dobrynin, S. S. Sheiko, *Science* **2018**, *359*, 1509.
[16] A. Miyamoto, S. Lee, N. F. Cooray, S. Lee, M. Mori, N. Matsuhisa, H. Jin, L. Yoda, T. Yokota, A. Itoh, M. Sekino, H. Kawasaki, T. Ebihara, M. Amagai, T. Someya, *Nat. Nanotechnol.* **2017**, *12*, 907.
[17] B. Sun, R. N. McCay, S. Goswami, Y. Xu, C. Zhang, Y. Ling, J. Lin, Z. Yan, *Adv. Mater.* **2018**, *30*, 1804327.
[18] Y. Xu, B. Sun, Y. Ling, Q. Fei, Z. Cheng, X. Li, P. Guo, N. Jeon, S. Goswami, Y. Liao, S. Ding, Q. Yu, J. Lin, G. Huang, Z. Yan, *Proc. Natl. Acad. Sci. U. S. A.* **2020**, *117*, 205.
[19] W. Zhou, S. Yao, H. Wang, Q. Du, Y. Ma, Y. Zhu, *ACS Nano* **2020**, *14*, 5798.
[20] S. Zheng, W. Li, Y. Ren, Z. Liu, X. Zou, Y. Hu, J. Guo, Z. Sun, F. Yan, *Adv. Mater.* **2022**, *34*, 2106570.
[21] J. H. Kim, S. R. Kim, H. J. Kil, Y. C. Kim, J. W. Park, *Nano Lett.* **2018**, *18*, 4531.
[22] S. H. Jeong, S. Zhang, K. Hjort, J. Hilborn, Z. Wu, *Adv. Mater.* **2016**, *28*, 5830.
[23] D. C. Kim, H. J. Shim, W. Lee, J. H. Koo, D. H. Kim, *Adv. Mater.* **2020**, *32*, 1902743.
[24] R. Ye, H. Xu, C. Wan, S. Peng, L. Wang, H. Wu, Z. P. Aguilar, Y. Xiong, Z. Zeng, H. Wei, *Biochem. Biophys. Res. Commun.* **2013**, *439*, 148.
[25] Y. Q. Li, Q. Han, J. L. Feng, W. L. Tian, H. Z. Mo, *Food Control* **2014**, *43*, 22.
[26] M. G. Dunn, F. H. Silver, D. A. Swann, *J. Invest. Dermatol.* **1985**, *84*, 9.
[27] K. Li, Y. Shuai, X. Cheng, H. Luan, S. Liu, C. Yang, Z. Xue, Y. Huang, Y. Zhang, *Small* **2022**, *18*, 2107879.
[28] Y. Xu, Z. Zhi, Q. Gao, M. Xie, M. Yu, B. Lei, P. Li, P. X. Ma, *Adv. Healthcare Mater.* **2017**, *6*, 1601173.
[29] S. S. Virani, A. Alonso, E. J. Benjamin, M. S. Bittencourt, C. W. Callaway, A. P. Carson, A. M. Chamberlain, A. R. Chang, S. Cheng, F. N. Delling, *Circulation* **2020**, *141*, e139.
[30] H. C. McGill Jr, C. A. McMahan, S. S. Gidding, *Circulation* **2008**, *117*, 1216.
[31] P. J. Zimetbaum, M. E. Josephson, *N. Engl. J. Med.* **2003**, *348*, 933.
[32] M. P. Turakhia, D. D. Hoang, P. Zimetbaum, J. D. Miller, V. F. Froelicher, U. N. Kumar, X. Xu, F. Yang, P. A. Heidenreich, *Am. J. Cardiol.* **2013**, *112*, 520.
[33] A. Y. Hannun, P. Rajpurkar, M. Haghpanahi, G. H. Tison, C. Bourn, M. P. Turakhia, A. Y. Ng, *Nat. Med.* **2019**, *25*, 65.
[34] A. Taebi, A. B. E. Solar, A. J. Bomar, R. H. Sandler, H. A. Mansy, *Vibration* **2019**, *2*, 64.
[35] Y. Liu, J. J. Norton, R. Qazi, Z. Zou, K. R. Ammann, H. Liu, L. Yan, P. L. Tran, K. Jang, J. W. Lee, D. Zhang, K. Kilian, S. Jung, T. Bretl, J. Xiao, M. Slepian, Y. Huang, J. Jeong, J. A. Rogers, *Sci. Adv.* **2016**, *2*, e1601185.
[36] M. Etemadi, O. T. Inan, *J. Appl. Physiol.* **2018**, *124*, 452.
[37] W. Lee, H. Kim, I. Kang, H. Park, J. Jung, H. Lee, H. Park, J. S. Park, J. M. Yuk, S. Ryu, J. Jeong, J. Kang, *Science* **2022**, *378*, 637.
[38] P. Li, Y. F. Poon, W. Li, H. Zhu, S. H. Yeap, Y. Cao, X. Qi, C. Zhou, M. Lamrani, R. W. Beuerman, E. Kang, Y. Mu, C. M. Li, M. W. Chang, S. S. J. Leong, M. B. Chan-Park, *Nat. Mater.* **2011**, *10*, 149.